

Article

# Pharmaceutical Salts of Enrofloxacin with Organic Acids

Hong Pang <sup>1</sup>, Yu-Bin Sun <sup>1</sup>, Jun-Wen Zhou <sup>1</sup>, Meng-Juan Xie <sup>1</sup>, Hao Lin <sup>1</sup>, Yan Yong <sup>2</sup>, Liang-Zhu Chen <sup>2</sup> and Bing-Hu Fang <sup>1,2,\*</sup>

<sup>1</sup> National Laboratory of Safety Evaluation (Environmental Assessment) of Veterinary Drugs, South China Agricultural University, Guangzhou 510000, China; pang\_h163@163.com (H.P.); 18826231020@163.com (Y.-B.S.); zhou\_j\_wen@163.com (J.-W.Z.); xie\_mjuan@163.com (M.-J.X.); 18319772187@163.com (H.L.)

<sup>2</sup> Guangdong Dahuanong Animal Health Products Co. Ltd., Yunfu 527400, China; xiaoyner@126.com (Y.Y.); che\_lizh@163.com (L.-Z.C.)

\* Correspondence: fangbh@scau.edu.cn

Received: 1 July 2020; Accepted: 24 July 2020; Published: 27 July 2020



**Abstract:** Enrofloxacin is a poorly soluble antibacterial drug of the fluoroquinolones class used in veterinary medicine. The main purpose of this work was to investigate the structural and pharmaceutical properties of new enrofloxacin salts. Enrofloxacin anhydrate and its organic salts with tartaric acid, nicotinic acid and suberic acid formed as pure crystalline anhydrous solids. All the crystals were grown from a mixed solution by slow evaporation at room temperature. These products were then characterized by field-emission scanning electron microscopy, powder X-ray diffraction, Fourier transform infrared spectroscopy and differential scanning calorimetry. Further, X-ray single crystal diffraction analysis was used to study the crystal structure. The intermolecular interactions and packing arrangements in the crystal structures were studied, and the solubility of these salts in water was determined using high-performance liquid chromatography. The results show that the new salts of enrofloxacin developed in this study exhibited excellent water solubility.

**Keywords:** enrofloxacin; salts; crystal structure; organic acids; solubility

## 1. Introduction

Crystal engineering through multicomponent crystals has attracted substantial attention in the pharmaceutical field in recent years [1,2] because of the possibility of improved solubility and bioavailability of newly designed drug compounds (polymorphs, salt and cocrystals) [3,4]. The formation of the salt/cocrystal is based on the crystal engineering concepts [5]. The salt/cocrystal formation provides an enormous scope for the manipulation and modification of crucial pharmaceutical physical properties such as the dissolution rate, solubility, thermodynamic stability and bioavailability [6,7]. Proton transfer is a decisive factor that distinguishes salts from cocrystals: In salt formation, proton transfer and ionization occur, while these do not occur in the formation of cocrystals [8]. Salts and cocrystals have been employed in the pharmaceutical industry because of their excellent solubility [9]. Although cocrystallization has many exciting advantages, salt formation still represents a widely accepted method to obtain higher solubility of the drug [10].

Most of the active pharmaceutical ingredients (APIs) available in the current market cause formulation difficulties because of poor water solubility, which may lead to poor oral bioavailability [11,12]. Hence, improving the solubility and bioavailability of APIs without changing their stability and other characteristics has become a challenging task. Notably, every crystal structure is the result of mutual balance between numerous noncovalent interactions, but the hydrogen

bond remains an important factor in supramolecular assembly [13]. The design of supramolecular heterosynthons derived from organic salts was hypothesized on the basis of the supramolecular synthon strategy in the context of crystal engineering [14,15]. Recently, this strategy has been effectively adopted in the field of pharmaceutical crystallization [16].

Enrofloxacin (1-cyclopropyl-7-(4-ethylpiperazin-1-yl)-6-fluoro-4-oxo-1,4-dihydroquinoline-3-carboxylate) shows a wide spectrum of antibacterial activity, and it belongs to the class of fluoroquinolone antibiotics [17]. As an important synthetic bacteriostatic drug, it has been widely used in stock raising. In good clinical trials, its effectiveness in treating uncomplicated and complicated urinary tract infections, urethral and cervical gonococcal infections, respiratory tract infections, and skin and tissue infections has been proven [18]. It exhibits concentration-dependent antibacterial activity [19]. Enrofloxacin exists in a zwitterionic form within a neutral aqueous solution due to the acid/base interaction between the basic nitrogen of the piperazine and the carboxylic acid group [20,21]. Therefore, in water at  $\text{pH} \approx 7$ , enrofloxacin exhibits a low solubility (0.45 mg/mL) [21]. In addition, low solubility of enrofloxacin is one of the unfavourable properties in formulation [22]. Therefore, a method to improve its solubility without compromising performance has been sought. A weak organic acid can be used as an organic counterionic component for salt formation [23,24]. These acids can potentially present the formation of salts with multiple stoichiometries due to the containment of carboxylic group. This approach is widely used in pharmaceutical industries to enhance solubility, bioavailability and controlled release of drugs [25]. Therefore, we adopted crystal engineering concepts to select pharmaceutically acceptable organic counterions to form salts with enrofloxacin.

In this study, we prepared enrofloxacin anhydrate and salt trihydrate with tartaric acid and salt solvate with nicotinic acid and suberic acid, and we analysed the crystal structures of these compounds. The obtained crystal compounds were characterized by field-emission scanning electron microscopy (FESEM), Fourier transform infrared spectroscopy (FT-IR), powder X-ray diffraction (PXRD) and differential scanning calorimetry (DSC). All the crystal structure data were successfully resolved by single-crystal X-ray diffraction (SCXRD), and the crystal conformations and packing arrangements were studied in detail. Finally, the solubility of the new phases in water was also determined by high-performance liquid chromatography (HPLC). The new salts were found to exhibit significantly improved solubility and were therefore suitable for use in drug formulation.

## 2. Experimental

### 2.1. Materials

Enrofloxacin ( $\text{C}_{19}\text{H}_{22}\text{FN}_3\text{O}_3$ , 98%) was obtained from Nanjing Kangmanlin Biomedical Technology Co. Ltd. (Nanjing, China). These organic acids (tartaric acid ( $\text{C}_4\text{H}_6\text{O}_6$ , 99.5%), nicotinic acid ( $\text{C}_6\text{H}_5\text{NO}_2$ , 99.5%), suberic acid ( $\text{C}_6\text{H}_{10}\text{O}_4$ , 99%)) were purchased from Shanghai Macklin Biochemical Co., Ltd. (Shanghai, China). The chromatography grade organic solvents (methanol (MeOH), acetonitrile (ACN), triethylamine (TEA), phosphate) were purchased from Tianjin Kemio Chemical Reagent Co., Ltd. (Tianjin, China). All of the analytical-grade organic solvents (ethanol (EtOH), dichloromethane (DCM), *N,N*-Dimethylformamide (DMF)) were obtained from Tianjin Damao Chemical Reagent Factory (Tianjin, China) and these were used without further purification. Purified water was prepared using the Millipore Milli-Q system.

### 2.2. Crystallization of Enrofloxacin Anhydrate

Enrofloxacin Anhydrate (**1**): Enrofloxacin (230 mg, 0.64 mmol) was added to 4 mL of an ethanol/dichloromethane mixed solvent (1:1 *v/v*) for crystallization. The **1** crystals in the suspension were then filtered and dried in air (yield: 77%).

### 2.3. Preparation of Salts and Crystallization

Enrofloxacin and various acids in equal molar ratios were dissolved in a mixed solvent in a 50-mL conical flask, and this mixture was stirred at 50 °C until a completely clear solution was obtained. The solution was then allowed to slowly evaporate at room temperature to obtain single crystals of the products. Diffraction-quality crystals were obtained within 1–5 days. Each sample was scaled up 20 times for the solubility determination.

Enrofloxacin Tartrate Trihydrate (**2**): A 1:1 mixture of enrofloxacin (460 mg, 1.28 mmol) and tartaric acid (180 mg, 1.28 mmol) was added to 12 mL of a water/ethanol/dichloromethane mixed solvent (4:7:3 *v/v/v*) for crystallization. Then, **2** was obtained by filtration and drying in air (yield: 76%).

Enrofloxacin Nicotinat-EtOH Salt Solvate (**3**): A 1:1 mixture of enrofloxacin (230 mg, 0.64 mmol) and nicotinic acid (83.7 mg, 0.64 mmol) was added to 5 mL of an ethanol/dichloromethane mixed solvent (3:2 *v/v*) for crystallization. The resulting **3** crystals were filtered and dried in air (yield: 86%).

Enrofloxacin Suberate-2EtOH Salt Solvate (**4**): A 1:1 mixture of enrofloxacin (230 mg, 0.64 mmol) and suberic acid (110 mg, 0.64 mmol) was added to 4 mL of an ethanol/dichloromethane mixed solvent (1:1 *v/v*) for crystallization. Crystals were then obtained by filtration and drying (yield: 77%).

### 2.4. Field-Emission Scanning Electron Microscopy (FESEM)

The surface morphology of the samples was investigated by FESEM (Heidelberg, Germany) using a Zeiss Sigma 300.

### 2.5. Powder X-ray Diffraction (PXRD)

PXRD measurements of the new compounds were carried out on a Rigaku-Ultima IV X-ray powder diffractometer (Tokyo, Japan) using Cu K $\alpha$  radiation ( $\lambda = 1.54178 \text{ \AA}$ ) at 40 kV and 40 mA. Samples were analysed in the  $2\theta$  range from 5° to 80° with a scanning rate of 8°/min. These data were collected at room temperature and analysed using Jade 6.0 software (Livermore, CA, USA).

### 2.6. Fourier Transform Infrared (FT-IR)

FT-IR spectra were collected using a Bruker Vertex 70 spectrometer and measured in the range of 4000–400  $\text{cm}^{-1}$  with an RT-DLaTGS detector (Ettlingen, Germany). The KBr diffuse-reflectance mode was used (sample concentration: 1 mg in 100 mg of KBr) for recording the IR spectra of these samples. Data were analysed using the OPUS software (San Francisco, CA, USA).

### 2.7. Single Crystal X-ray Diffraction (SCXRD)

X-ray diffraction data were collected using a Rigaku Oxford Diffraction SuperNova diffractometer (Oxford, UK) equipped with a monochromator mirror for Cu K $\alpha$  ( $\lambda = 1.54184 \text{ \AA}$ ) radiation at 150 K. Data reduction was carried out using the CrysAlisPro software, and absorption correction was implemented in the SCALE3 ABSPACK scaling algorithm. The structure was solved (direct methods) and refined (using least squares minimization) with Olex2 [26] using SHELX [27] structure solution programs. All the non-H atoms were refined anisotropically. In addition, all the figures, including the packing and molecular structure diagrams, were drawn using Olex2 and PLATON [28]. Table 1 gives the pertinent crystallographic data, and Table 2 gives the hydrogen-bond parameters.

**Table 1.** Crystallographic Data for Compounds 1–4.

Crystal Parameters	1	2	3	4
Empirical formula	C <sub>19</sub> H <sub>22</sub> FN <sub>3</sub> O <sub>3</sub>	C <sub>23</sub> H <sub>31</sub> FN <sub>3</sub> O <sub>10.5</sub>	C <sub>27</sub> H <sub>33</sub> FN <sub>4</sub> O <sub>6</sub>	C <sub>29</sub> H <sub>42</sub> FN <sub>3</sub> O <sub>8</sub>
Formula weight	359.39	536.51	528.57	579.65
Temperature/K	150.03(12)	150.00(10)	150.00(10)	150.00(10)
Crystal system	monoclinic	triclinic	triclinic	triclinic
Space group	<i>P</i> 2 <sub>1</sub> / <i>n</i>	<i>P</i> $\bar{1}$	<i>P</i> $\bar{1}$	<i>P</i> $\bar{1}$
<i>a</i> /Å	13.9309(2)	7.4444(4)	8.4841(4)	6.9755(2)
<i>b</i> /Å	6.87600(10)	11.2932(6)	12.1821(6)	9.3315(4)
<i>c</i> /Å	18.5133(3)	15.5835(9)	13.6436(6)	23.4431(9)
$\alpha$ /°	90	86.475(4)	115.392(4)	99.065(3)
$\beta$ /°	100.9240(10)	77.366(4)	93.462(4)	95.004(3)
$\gamma$ /°	90	74.427(5)	92.054(4)	104.306(3)
Volume/Å <sup>3</sup>	1741.23(5)	1231.46(12)	1268.59(11)	1447.42(10)
<i>Z</i>	4	2	2	2
$\rho_{\text{calc}}$ /cm <sup>3</sup>	1.371	1.447	1.384	1.330
$\mu$ /mm <sup>-1</sup>	0.839	1.023	0.861	0.841
<i>F</i> (000)	760.0	566.0	560.0	620.0
Crystal size/mm <sup>3</sup>	0.7 × 0.4 × 0.4	0.2 × 0.02 × 0.01	0.4 × 0.3 × 0.25	0.25 × 0.15 × 0.03
Radiation	CuK $\alpha$ ( $\lambda$ = 1.54184)	CuK $\alpha$ ( $\lambda$ = 1.54184)	CuK $\alpha$ ( $\lambda$ = 1.54184)	CuK $\alpha$ ( $\lambda$ = 1.54178)
2 $\theta$ range for data collection/°	7.314 to 146.554	8.128 to 148.07	7.198 to 134.982	7.704 to 137.998
Index ranges	−13 ≤ <i>h</i> ≤ 17, −8 ≤ <i>k</i> ≤ 5, −22 ≤ <i>l</i> ≤ 20	−9 ≤ <i>h</i> ≤ 9, −14 ≤ <i>k</i> ≤ 11, −19 ≤ <i>l</i> ≤ 19	−10 ≤ <i>h</i> ≤ 9, −14 ≤ <i>k</i> ≤ 14, −16 ≤ <i>l</i> ≤ 14	−7 ≤ <i>h</i> ≤ 8, −11 ≤ <i>k</i> ≤ 11, −28 ≤ <i>l</i> ≤ 27
Reflections collected	5229	8302	6853	10,171
Independent reflections	3299 [R <sub>int</sub> = 0.0297, R <sub>sigma</sub> = 0.0325]	4827 [R <sub>int</sub> = 0.0317, R <sub>sigma</sub> = 0.0427]	4494 [R <sub>int</sub> = 0.0339, R <sub>sigma</sub> = 0.0366]	5318 [R <sub>int</sub> = 0.0262, R <sub>sigma</sub> = 0.0340]
Data/restraints/parameters	3299/0/238	4827/0/369	4494/0/348	5318/72/462
Goodness-of-fit on F <sup>2</sup>	1.062	1.030	1.054	1.018
Final R indexes [ <i>I</i> >= 2 $\sigma$ ( <i>I</i> )]	R <sub>1</sub> = 0.0509, wR <sub>2</sub> = 0.1325	R <sub>1</sub> = 0.0483, wR <sub>2</sub> = 0.1236	R <sub>1</sub> = 0.0532, wR <sub>2</sub> = 0.1475	R <sub>1</sub> = 0.0695, wR <sub>2</sub> = 0.1736
Final R indexes [all data]	R <sub>1</sub> = 0.0528, wR <sub>2</sub> = 0.1355	R <sub>1</sub> = 0.0580, wR <sub>2</sub> = 0.1307	R <sub>1</sub> = 0.0585, wR <sub>2</sub> = 0.1531	R <sub>1</sub> = 0.0792, wR <sub>2</sub> = 0.1838
Largest diff. peak/hole/e Å <sup>-3</sup>	0.25/−0.40	0.36/−0.42	0.76/−0.56	0.45/−0.49
CCDC	2000796	2000797	2000798	2000799

**Table 2.** Hydrogen Bond Geometry Parameters in Compounds 1–4.

D–H...A	D...A (Å)	H...A (Å)	D–H...A (Deg)
<b>Compound 1</b>			
O1–H1...O3	2.5460(14)	1.78	154
C2–H2...O2	2.7950(16)	2.46	101
C8–H8A...O1	3.4690(16)	2.56	157
C8–H8B...O3	3.2816(16)	2.33	167
C9–H9...O3	3.2232(15)	2.45	135
C15–H15B...F1	2.8895(15)	2.24	123
<b>Compound 2</b>			
O1–H1...O3	2.5182(19)	1.76	153
N3–H3...O7	3.022(2)	2.21	139
N3–H3...O9	2.835(2)	1.99	142
O6–H6...O4	2.624(3)	2.15	117
O6–H6...O11	3.051(12)	2.37	141

Table 2. Cont.

D–H...A	D...A (Å)	H...A (Å)	D–H...A (Deg)
O6–H6...O12	3.097(13)	2.37	148
O7–H7...O5	2.610(2)	1.80	171
O8–H8...O4	2.439(3)	1.29(5)	174(4)
O10–H10A...O6	2.684(4)	1.90	154
O10–H10B...O2	2.805(3)	2.00	158
O11–H11A...O6	3.051(12)	2.47	126
O11–H11A...O7	3.367(12)	2.54	165
O11–H11B...O4	2.870(11)	2.40	116
O11–H11B...O9	2.909(12)	2.12	153
O12–H12A...O11	2.823(15)	2.00	164
O12–H12A...O12	2.715(16)	1.90	160
O12–H12B...O4	2.985(10)	2.50	117
O12–H12B...O9	3.057(13)	2.25	158
C2–H2...O2	2.836(2)	2.53	100
C7–H7B...O2	3.567(3)	2.60	175
C9–H9...O3	3.306(3)	2.38	157
C10–H10...O3	3.411(3)	2.51	163
C14–H14A...O8	3.325(2)	2.39	162
C15–H15A...F1	2.872(2)	2.22	123
C17–H17A...O1	3.165(2)	2.25	156
C18–H18B...O6	3.015(3)	2.55	109
C19–H19A...O7	3.343(3)	2.56	139
C19–H19A...O11	3.194(13)	2.46	133
C21–H21...O8	2.884(3)	2.51	102
<b>Compound 3</b>			
O1–H1...O3	2.536(2)	1.77	154
N3–H3...O4	2.618(2)	1.64	172
O6–H6...O5	2.761(3)	1.94	178
C2–H2...O2	2.799(3)	2.48	101
C8–H8B...O3	3.363(3)	2.45	157
C14–H14B...O6	3.460(3)	2.54	158
C15–H15A...F1	2.861(3)	2.22	123
C16–H16A...O4	3.241(2)	2.48	135
C17–H17A...O3	3.349(2)	2.52	144
C18–H18B...O2	3.224(3)	2.44	138
C23–H23...O4	2.792(3)	2.46	101
<b>Compound 4</b>			
O1–H1...O3	2.740(12)	1.95	162
N3–H3...O6	2.667(3)	1.74	155
O5–H5...O6	2.567(3)	1.75	174
O8–H8...O7	2.731(6)	1.94	162
C2–H2...O2	2.723(9)	2.27	109
C7–H7A...F1	3.430(8)	2.46	174
C8–H8A...O8	3.040(8)	2.59	108
C9–H9...O3	3.347(7)	2.57	137
C15–H15A...F1	2.882(3)	2.26	121
C16–H16B...O1	3.358(10)	2.44	158
C16–H16B...O1A	3.435(8)	2.49	166
C17–H17B...O4	3.320(3)	2.39	161
C29–H29B...O1A	3.203(10)	2.53	127

### 2.8. Differential Scanning Calorimetry (DSC)

Thermal analyses of these samples were performed on a DSC (Q200 V24.10 Build 122) instrument (New Castle, DE, USA): 2–3 mg of the crystals was placed in standard aluminium pans and scanned at 20 °C/min in the range 25–280 °C under a nitrogen gas flow of 50 mL/min. Data were analysed using the Universal Analysis 2000 software (New Castle, DE, USA).

### 2.9. Solubility Analyses

The solubility of these products was determined according to the shake-flask method [29]. Excess amounts (100 mg) of the crystals were added to the screw-capped glass vials containing

2.5 mL of ultrapure water, and the resulting suspensions was shaken at room temperature. After 24 h, the suspensions were filtered through 0.22- $\mu\text{m}$  polycarbonate filters, and the compounds' concentrations were determined using the Agilent 1260 Infinity II HPLC system (Palo Alto, CA, USA) equipped with a 1260 Multi  $\lambda$  Fluorescence detector with the wavelength of the excited and emitted spectra of crystals being 280 nm and 450 nm, respectively. The C18 HPLC column (Poroshell 120 EC-C18, 4.6 mm  $\times$  100 mm, 2.7  $\mu\text{m}$ ) was employed, and acetonitrile, methanol and triethylamine phosphate (pH = 2.5) were used as the mobile phase (1:24:75, *v:v::v*) with a flow rate of 1 mL/min. Each solubility test was performed in triplicate.

### 3. Results and Discussion

#### 3.1. Field-Emission Scanning Electron Microscopy (FESEM)

The FESEM (Heidelberg, Germany) images provide information about the crystal morphology of several new crystals (Figure 1). Needle-shaped or long rod-shaped forms are seen for the products 1 and 2, whereas 3 and 4 displayed rectangular blocks and fragmentary crystals.

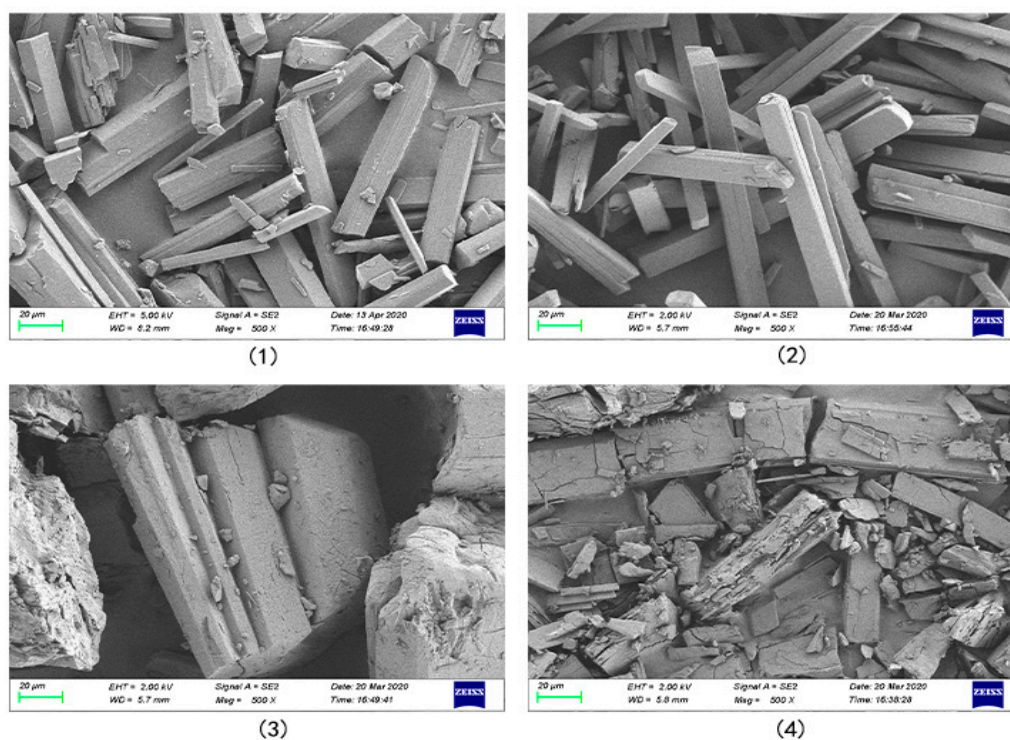


**Figure 1.** Field-emission scanning electron microscopy (FESEM) photos of compounds 1–4.

#### 3.2. PXRD Analysis

PXRD enables the study and characterization of novel crystalline materials [30]. PXRD patterns of the four crystal samples are shown in Figure 2. The patterns for 1 were different from those of the starting material and from the previously published PXRD patterns for the polymorphic form [31]. The purity of all products was confirmed by comparing the PXRD patterns with the simulated patterns obtained from the single crystal data (see the Supplementary Materials, Figures S1–S4). No apparent peaks corresponding to impurities were observed, so the obtained powder compounds were considered to be of high chemical purity. Further, these PXRD patterns of enrofloxacin compounds 2–4 differ significantly from the patterns of individual APIs, proving the formation of the new crystalline phases.

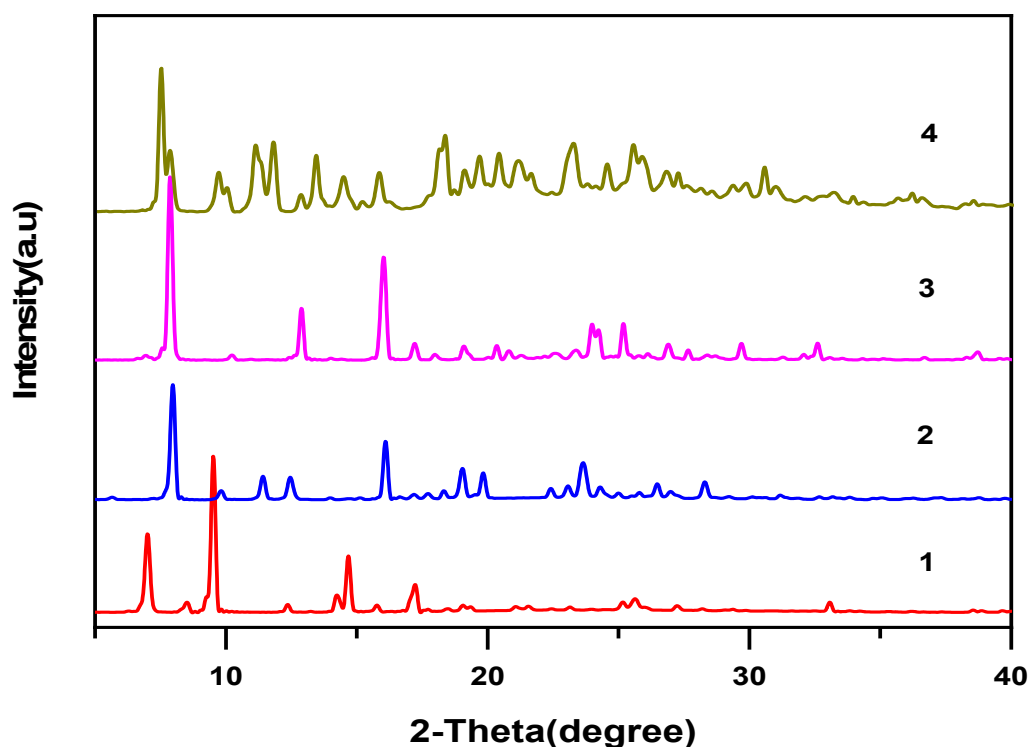


Figure 2. Powder X-ray diffraction (PXRD) patterns of compounds 1–4.

### 3.3. Spectroscopic Characterization

The FTIR analysis results for the products are given in Figure 3. The absorption band of crystalline enrofloxacin was located at  $1737\text{ cm}^{-1}$  because of the carbonyl stretching of its unionized carboxylic acid C=O group [31]. The C=O band in **1** was at  $1736.4\text{ cm}^{-1}$ , which indicates that the enrofloxacin exists as a neutral molecule. Slight peak shifts were also seen in compounds **2–4**, in particular, for the carboxylic acid C=O stretching, which shifted to  $1728.8\text{ cm}^{-1}$ ,  $1728.5\text{ cm}^{-1}$  and  $1729.3\text{ cm}^{-1}$ , respectively. This can be attributed to intermolecular interactions such as the formation of hydrogen bonds [32]. The terminal amino group of the piperazine ring was protonated in the process of crystallization, and this is proved by the presence of broad bands from  $2600\text{ cm}^{-1}$  to  $3000\text{ cm}^{-1}$ . However, confirming this is difficult because the broad IR absorption bands possibly overlap with others, e.g., in the case of the C–H stretching [33]. However, Karanam et al. reported FTIR analysis results that showed that enrofloxacin salts were protonated in the process of crystallization [34]. The medium-intensity broad band in the region of  $3300\text{–}3500\text{ cm}^{-1}$  is attributed to the O–H stretching of the water molecule **2** and ethanol molecule **3–4**. The existence of enrofloxacin as a neutral molecular and in the ionic state in the crystal structures was confirmed by SCXRD analysis.

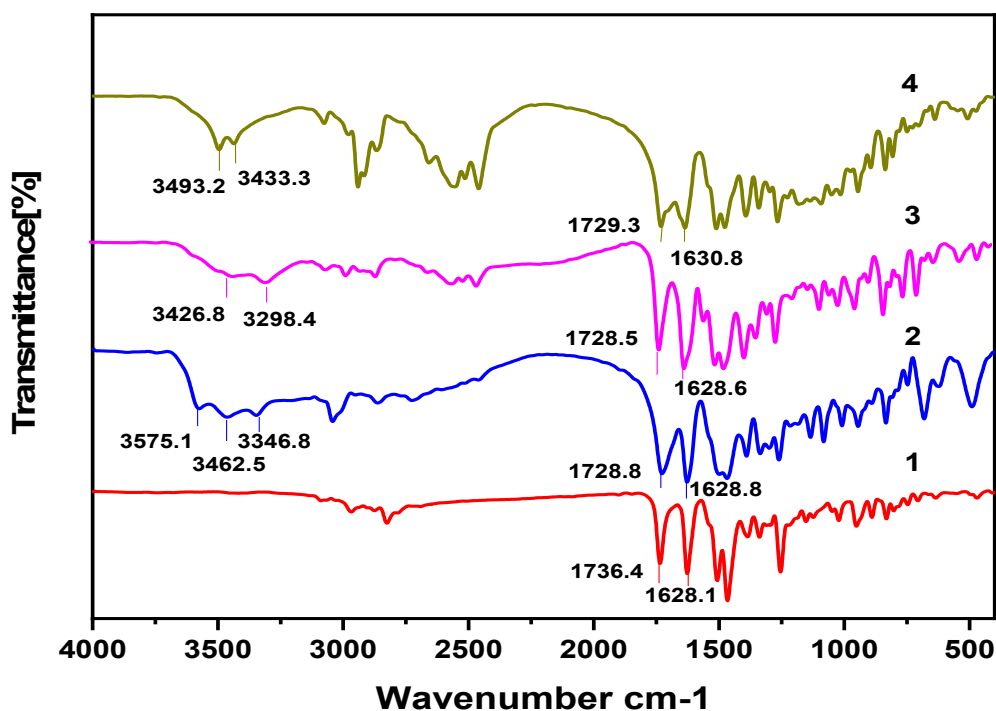
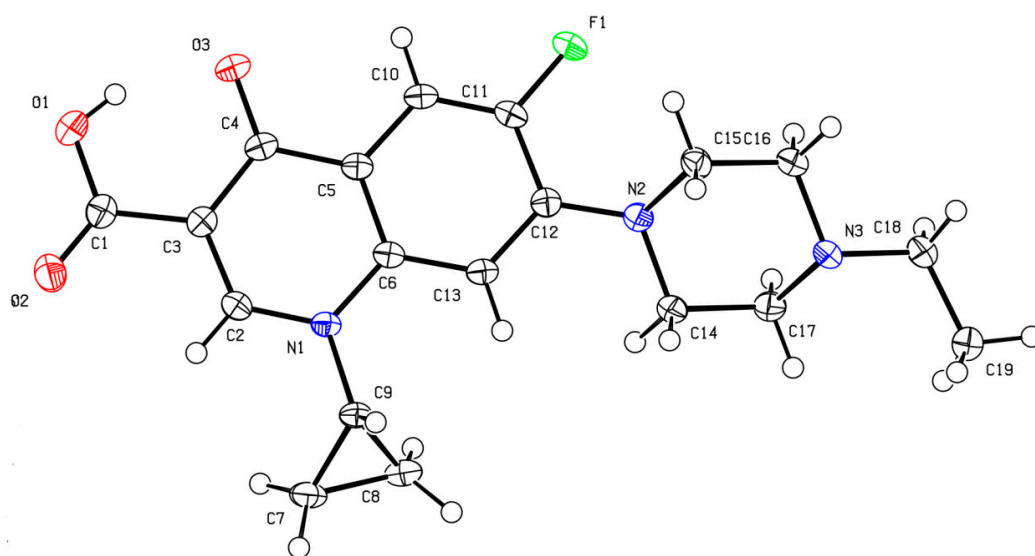


Figure 3. Fourier transform infrared (FTIR) spectrum of compounds 1–4.

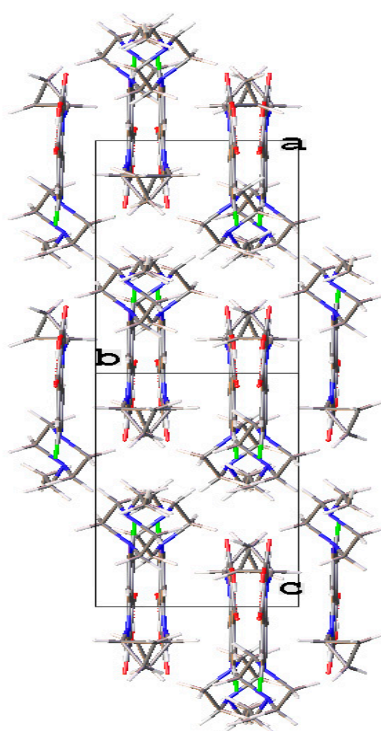
### 3.4. Crystal Structure Analysis

#### 3.4.1. Crystallization of Enrofloxacin Anhydrate (1)

Single crystals suitable for X-ray diffraction were obtained to determine the structures of the anhydrous form with a neutral molecule (no proton transfer from carboxylic acid to piperazinyl N atom; Figure 4a). The enrofloxacin anhydrate crystallized in the monoclinic  $P2_1/n$  space group with one molecule in the asymmetric unit. In addition, the piperazine ring in enrofloxacin usually exhibits a stable chair conformation with a torsion angle of  $C12-N2-C15-C16 = 158.25^\circ$ . It has the same crystal structure compared with the previous published [34]. The carboxylic acid group participated in intramolecular  $O-H\cdots O$  hydrogen bonding with the carbonyl oxygen atom of the quinolone moiety. The crystal structure was stacked with  $\pi\cdots\pi$  ( $3.598 \text{ \AA}$ ) interactions and was further stabilized by weak  $C-H\cdots O$  and  $C-H\cdots F$  hydrogen bonds Table 2 in enrofloxacin (Figure 4b).



(a)



(b)

**Figure 4.** (a) The molecular structure diagram of the product **1** (ellipsoids were drawn at the 50% probability level). (b) Molecular packing projections for product **1** along the [101] direction.

#### 3.4.2. Enrofloxacin Tartrate Trihydrate (**2**)

The novel enrofloxacin salt trihydrate **2** crystallized in the triclinic  $P\bar{1}$  space group. The 1:1 salt structure of enrofloxacin tartrate trihydrate contains an enrofloxacin cation, a tartrate anion and three  $H_2O$  molecules in the asymmetric unit (Figure 5a). One of the carboxylic acid groups of tartaric acid transferred one proton to the piperazinyl-ring N atom of the enrofloxacin molecule, resulting in a tartrate anion and enrofloxacin cation in the crystal structure (Figure 5b). The carboxylic acid group of enrofloxacin was involved in intramolecular O–H...O hydrogen bonding with the quinolone

oxygen atom. The product 2 displayed a unique hydrogen-bonding pattern with the formation of multicomponent crystals. The enrofloxacin cation interacted with the tartrate ion via  $N^+ - H \cdots O$  interactions to form the crystal structure, rather than forming hydrogen bonds with ionized oxygen atoms. Further, one of the water molecules connected the enrofloxacin cation and tartrate anion via  $O - H \cdots O$  interactions (Figure 5c).

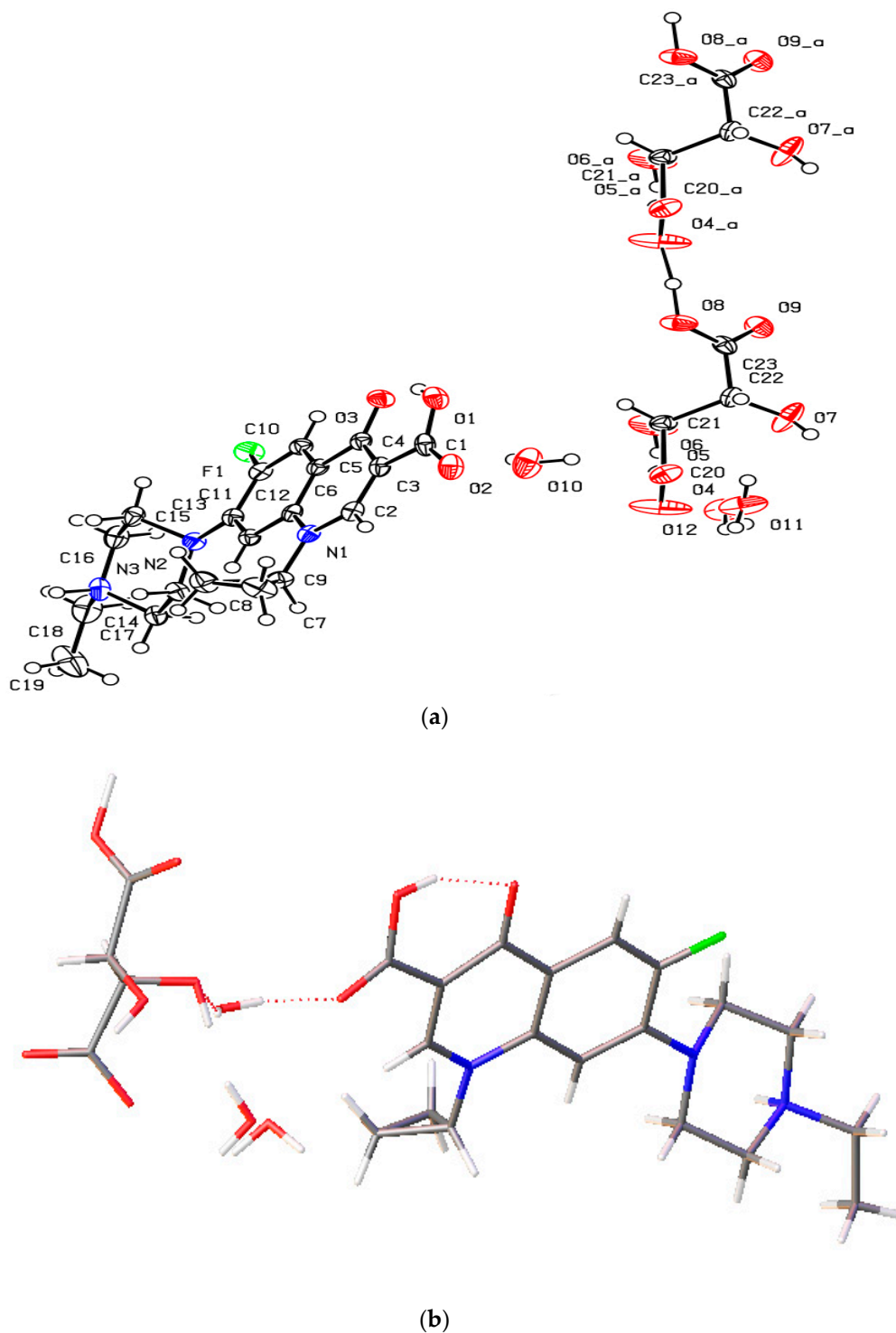
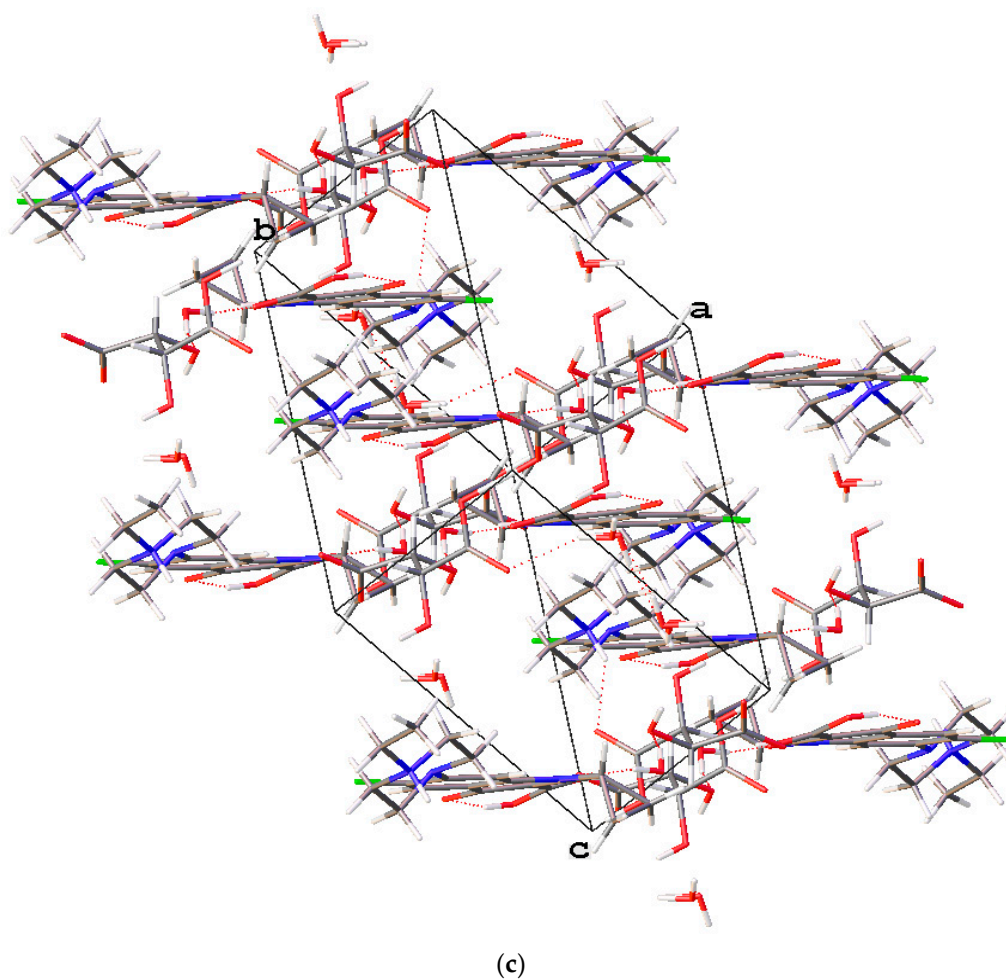


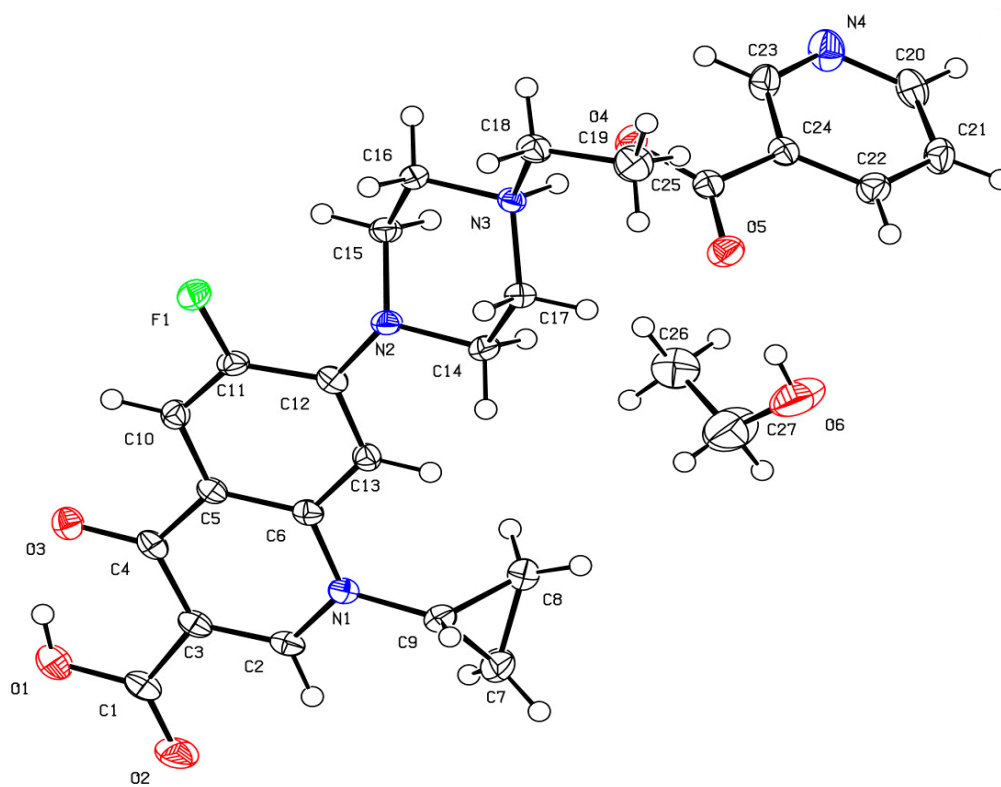
Figure 5. Cont.



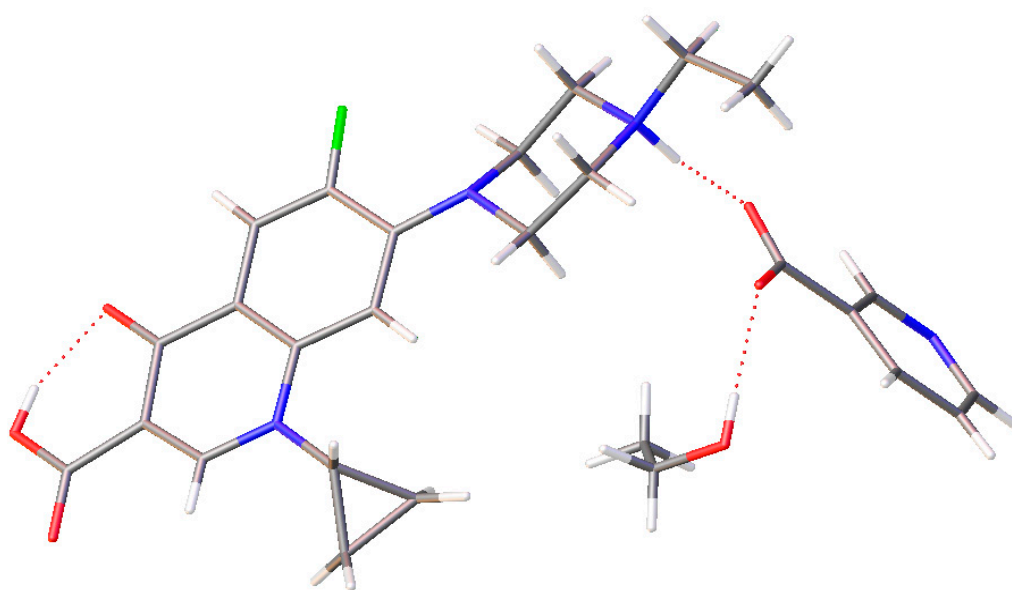
**Figure 5.** (a) The molecular structure diagram of the salt trihydrate **2** (ellipsoids were drawn at the 50% probability level). (b) Interaction between enrofloxacin and tartaric acid molecules in the crystal via O–H...O hydrogen bonds. (c) Molecular packing projections for salt trihydrate **2** along the [111] direction.

### 3.4.3. Enrofloxacin Nicotinate-EtOH Salt Solvate (**3**)

The novel enrofloxacin salt solvate **3** had a triclinic system and space group  $P\bar{1}$ . Its crystal contained an enrofloxacin cation, a nicotinate anion and an EtOH molecule in the asymmetric unit (Figure 6a). The carboxylic acid group of **3** was involved in intramolecular O–H...O hydrogen bonding with the quinolone oxygen atom. The nicotinic acid was ionized by proton transfer to the enrofloxacin molecule to form  $N^+–H...O^-$ , while the EtOH molecule formed the O–H...O hydrogen bond with the carboxylic acid C=O group of nicotinate (Figure 6b). The quinolone moieties of the enrofloxacin molecules stacked via  $\pi\cdots\pi$  (3.538 Å) interactions (Figure 6c).



(a)



(b)

Figure 6. Cont.

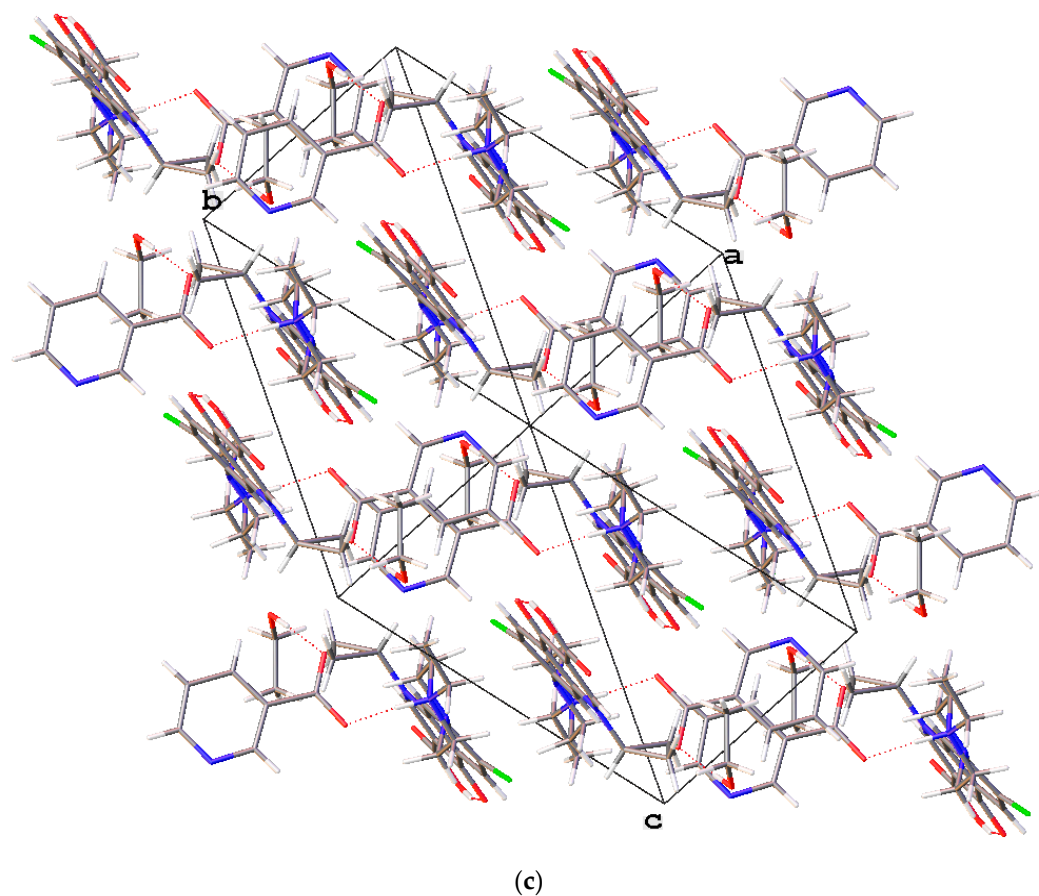


**Figure 6.** (a) The molecular structure diagram of the salt solvate 3 (ellipsoids were drawn at the 50% probability level). (b) Interaction between enrofloxacin and nicotinic acid molecules in the crystal via  $N^+ - H \cdots O^-$  and  $O - H \cdots O$  hydrogen bonds. (c) Molecular packing projections for salt solvate 3 along the [111] direction.

#### 3.4.4. Enrofloxacin Suberate-2EtOH Salt Solvate (4)

The novel enrofloxacin salt solvate 4 had a triclinic system and space group  $P\bar{1}$  with an enrofloxacin cation, a suberate anion and two EtOH molecules in the asymmetric unit. The carboxylic acid and cyclopropyl groups of the enrofloxacin molecule were observed to exhibit disorder in this crystal structure (Figure 7a). One of the carboxylic acid groups of the suberic acid transferred one proton to the piperazinyl-ring N atom of the enrofloxacin molecule, thereby forming a suberate anion and enrofloxacin cations in the crystal structure (Figure 7b). The carboxylic acid group of 4 was involved in intramolecular  $O - H \cdots O$  hydrogen bonding with the quinolone oxygen atom. Enrofloxacin interacted with the suberate ion via  $N^+ - H \cdots O^-$  interactions in the crystal structure, while the EtOH molecule formed the  $O - H \cdots O$  hydrogen bond with the carboxylic acid  $C=O$  group of the suberate ion. The quinolone moieties of the enrofloxacin molecule stacked via  $\pi \cdots \pi$  (3.872 Å) interactions (Figure 7c).

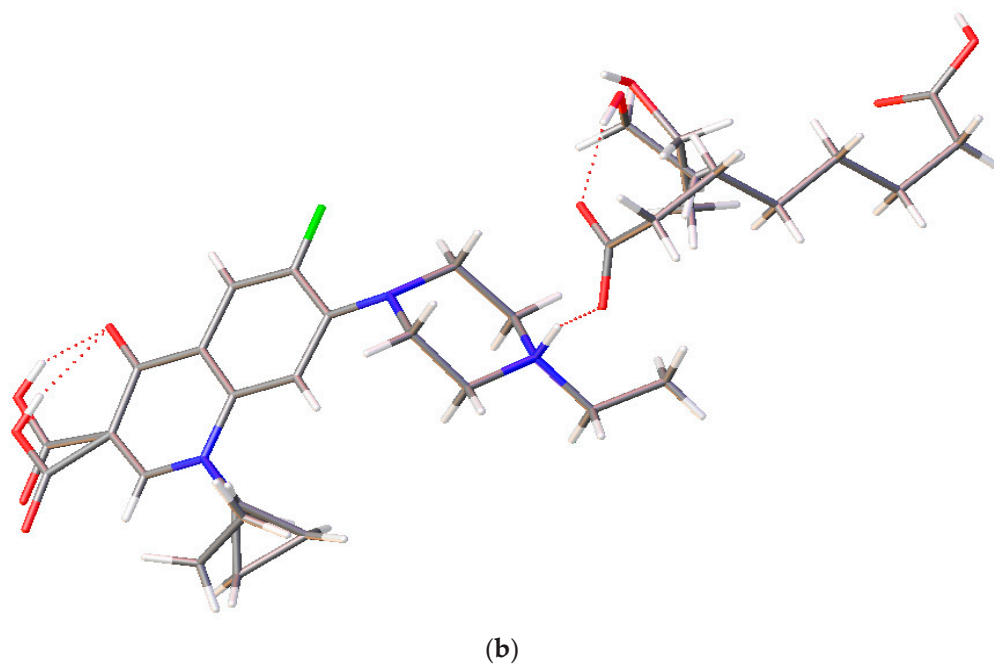
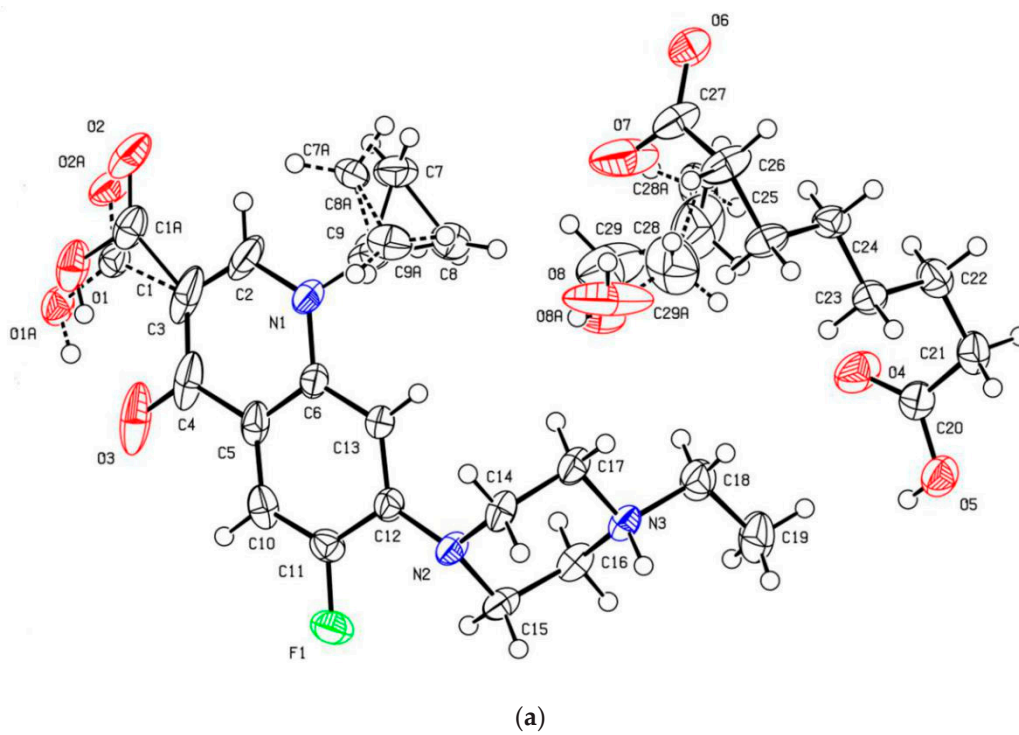
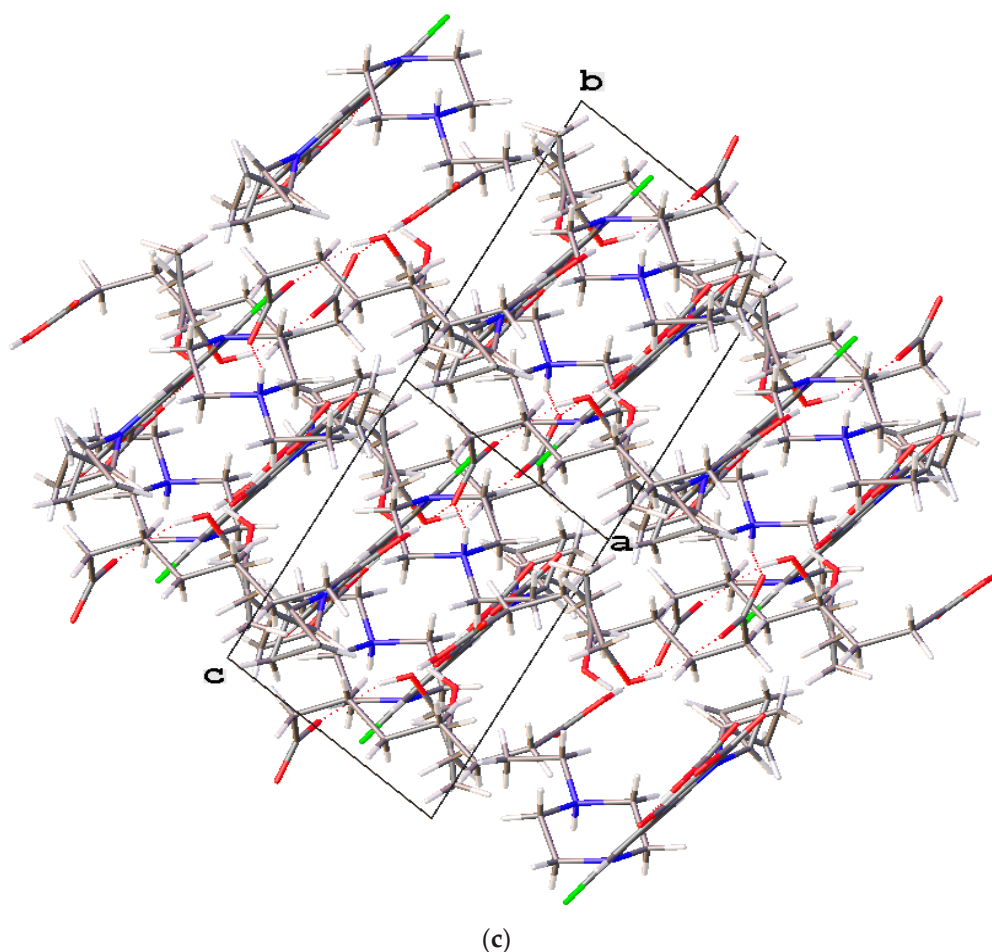


Figure 7. Cont.



**Figure 7.** (a) The molecular structure diagram of the salt solvate 4 (ellipsoids were drawn at the 50% probability level). (b) Interaction between enrofloxacin and suberic acid molecules in the crystal by  $N^+ - H \cdots O^-$  and  $O - H \cdots O$  hydrogen bonds. (c) Molecular packing projections for salt solvate 4 along the [011] direction.

### 3.5. Thermal Analysis

DSC curves showing the thermal behaviour of the products 1–4 are shown in Figure 8. The endothermic peak for melting of 1 was found at 228 °C. In the case of 2, the endothermic melting peak was at 228 °C, and this was followed by a phase transition. The endothermic transitions between 75 °C and 125 °C in the DSC thermograms for 2 showed the loss of water molecules from the crystal structure. In the DSC thermogram for 3, several steps of small endothermic transitions at about 120–180 °C due to solvent loss were observed, followed by a four-step endothermic melting transition of the salt solvate. Further, 4 was found to melt at 112 °C.

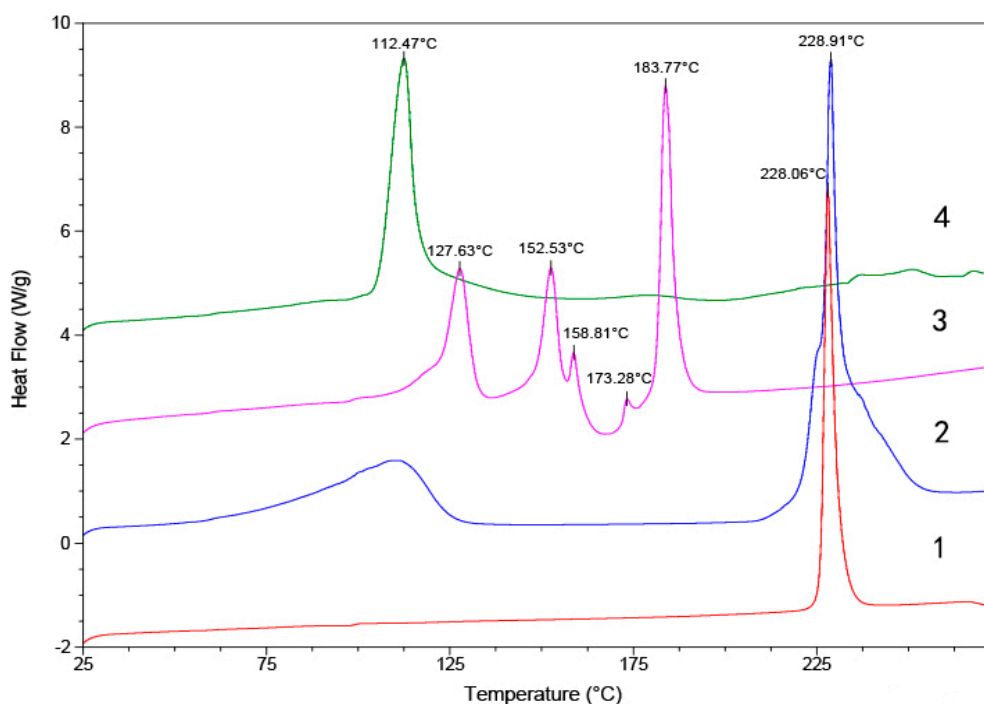


**Figure 8.** Differential scanning calorimetry (DSC) diagrams of compounds 1–4.

### 3.6. Results for Solubility Study

The solubility data are presented in Table 3. The solubility of commercially available enrofloxacin in water was 0.14 mg/mL, which is similar to the previously reported values [21]. The solubilities of 1 and the commercially available enrofloxacin are similar. As expected, the enrofloxacin salts showed a considerable improvement in solubility: 2–4 were found to be 57- to 406-times more soluble than pure enrofloxacin. Correlating the solubility with crystal structures is difficult because the limited experimental/calculated data on crystal packing, etc. However, it can be speculated that the solubility enhancement in the case of the salts was a result of greater ionization.

**Table 3.** Solubility Data for Compounds 1–4.

Compound	Saturation Solubility <sup>a</sup> in Water (mg/mL)
enrofloxacin <sup>b</sup>	0.14
1	0.14
2	8.53
3	56.83
4	8.04

<sup>a</sup> Solubility measured after 24 h of equilibration. <sup>b</sup> Solubility of commercially available enrofloxacin.

## 4. Discussion

Enrofloxacin anhydrate was crystallized, and the crystal structure was determined. Further, new salts formed using tartaric acid, nicotinic acid and suberic acid have been reported for the first time. The novel salts were prepared efficiently via evaporation using a mixed solvent has been found to be highly rewarding. These compounds formed a layered structure, and these layers were stacked via hydrogen bonds and  $\pi\cdots\pi$  interactions. In the structure of salts, the piperazinyl moieties of enrofloxacin interacted with the carboxylate ions. These carboxylate ions connected the H<sub>2</sub>O and EtOH molecules formed a stacking structure. The enrofloxacin salts prepared in this study showed a 57- to 406-fold higher solubility than the starting material.

**Supplementary Materials:** The following are available online at <http://www.mdpi.com/2073-4352/10/8/646/s1>. The PXRD patterns with the simulated patterns obtained from the single crystal data.CIF files giving crystal data can be obtained free of charge from the Cambridge Crystallographic Data Centre via the Internet [www.ccdc.cam.ac.uk/data\\_request/cif](http://www.ccdc.cam.ac.uk/data_request/cif).

**Author Contributions:** Writing—original draft, H.P.; Conceptualization, Y.-B.S.; Formal analysis, Y.Y., and L.-Z.C.; Funding acquisition, B.-H.F.; Investigation, J.-W.Z.; Methodology, M.-J.X.; Software, H.L. All authors have read and agreed to the published version of the manuscript.

**Funding:** This research was funded by the Natural Science Foundation of China (No. 31872522).

**Conflicts of Interest:** There are no conflict to declare.

## References

1. Vishweshwar, P.; McMahon, J.A.; Peterson, M.L.; Hickey, M.B.; Shattock, T.R.; Zaworotko, M.J. Crystal engineering of pharmaceutical co-crystals from polymorphic active pharmaceutical ingredients. *Chem. Commun.* **2005**, *36*, 4601. [[CrossRef](#)] [[PubMed](#)]
2. Maeno, Y.; Fukami, T.; Kawahata, M.; Yamaguchi, K.; Tagami, T.; Ozeki, T.; Suzuki, T.; Tomono, K. Novel pharmaceutical cocrystal consisting of paracetamol and trimethylglycine, a new promising cocrystal former. *Int. J. Pharmaceut.* **2014**, *473*, 179–186. [[CrossRef](#)]
3. Blagden, N.; de Matas, M.; Gavan, P.T.; York, P. Crystal engineering of active pharmaceutical ingredients to improve solubility and dissolution rates. *Adv. Drug Deliv. Rev.* **2007**, *59*, 617–630. [[CrossRef](#)] [[PubMed](#)]
4. McNamara, D.P.; Childs, S.L.; Giordano, J.; Iarriccio, A.; Cassidy, J.; Shet, M.S.; Mannion, R.; O'Donnell, E.; Park, A. Use of a Glutaric Acid Cocrystal to Improve Oral Bioavailability of a Low Solubility API. *Pharm. Res. Dordr.* **2006**, *23*, 1888–1897. [[CrossRef](#)]
5. Jones, W.; Motherwell, W.D.S.; Trask, A.V. Pharmaceutical Cocrystals: An Emerging Approach to Physical Property Enhancement. *MRS Bull.* **2006**, *11*, 875–879. [[CrossRef](#)]
6. Thakuria, R.; Delori, A.; Jones, W.; Lipert, M.P.; Roy, L.; Rodríguez-Hornedo, N. Pharmaceutical cocrystals and poorly soluble drugs. *Int. J. Pharm.* **2013**, *453*, 101–125. [[CrossRef](#)] [[PubMed](#)]
7. Darwish, S.; Zeglinski, J.; Krishna, G.R.; Shaikh, R.; Khraisheh, M.; Walker, G.M.; Croker, D.M. A New 1:1 Drug-Drug Cocrystal of Theophylline and Aspirin: Discovery, Characterization, and Construction of Ternary Phase Diagrams. *Cryst. Growth Des.* **2018**, *18*, 7526–7532. [[CrossRef](#)]
8. Aakeröy, C.B.; Fasulo, M.E.; Desper, J. Cocrystal or Salt: Does It Really Matter? *Mol. Pharm.* **2007**, *4*, 317–322. [[CrossRef](#)]
9. Basavoju, S.; Boström, D.; Velaga, S.P. Pharmaceutical Cocrystal and Salts of Norfloxacin. *Cryst. Growth Des.* **2006**, *6*, 2699–2708. [[CrossRef](#)]
10. Berge, S.M.; Bighley, L.D.; Monkhouse, D.C. Pharmaceutical salts. *J. Pharm. Sci.* **1977**, *66*, 1–19. [[CrossRef](#)]
11. Datta, S.; Grant, D.J.W. Crystal structures of drugs: Advances in determination, prediction and engineering. *Nat. Rev. Drug Discov.* **2004**, *3*, 42–57. [[CrossRef](#)] [[PubMed](#)]
12. Meyer, M.C. Drug Product Selection—Part 2: Scientific basis of bioavailability and bioequivalence testing. *Am. Pharm.* **1991**, *NS31*, 47–52. [[CrossRef](#)]
13. Fleischman, S.G.; Kuduva, S.S.; McMahon, J.A.; Moulton, B.; Bailey Walsh, R.D.; Rodríguez-Hornedo, N.; Zaworotko, M.J. Crystal Engineering of the Composition of Pharmaceutical Phases: Multiple-Component Crystalline Solids Involving Carbamazepine. *Cryst. Growth Des.* **2003**, *3*, 909–919. [[CrossRef](#)]
14. Childs, S.L.; Chyall, L.J.; Dunlap, J.T.; Smolenskaya, V.N.; Stahly, B.C.; Stahly, G.P. Crystal Engineering Approach to Forming Cocrystals of Amine Hydrochlorides with Organic Acids. Molecular Complexes of Fluoxetine Hydrochloride with Benzoic, Succinic, and Fumaric Acids. *J. Am. Chem. Soc.* **2004**, *126*, 13335–13342. [[CrossRef](#)]
15. Bis, J.A.; Zaworotko, M.J. The 2-Aminopyridinium-carboxylate Supramolecular Heterosynthon: A Robust Motif for Generation of Multiple-Component Crystals. *Cryst. Growth Des.* **2005**, *5*, 1169–1179. [[CrossRef](#)]
16. Douroumis, D.; Ross, S.A.; Nokhodchi, A. Advanced methodologies for cocrystal synthesis. *Adv. Drug Deliv. Rev.* **2017**, *117*, 178–195. [[CrossRef](#)]
17. Efthimiadou, E.K.; Katsaros, N.; Karaliota, A.; Psomas, G. Synthesis, characterization, antibacterial activity, and interaction with DNA of the vanadyl-enrofloxacin complex. *Bioorg. Med. Chem. Lett.* **2007**, *17*, 1238–1242. [[CrossRef](#)]

18. Fan, J.; Sun, D.; Yu, H.; Kerwin, S.M.; Hurley, L.H. Self-Assembly of a Quinobenzoxazine-Mg<sup>2+</sup> Complex on DNA: A New Paradigm for the Structure of a Drug-DNA Complex and Implications for the Structure of the Quinolone Bacterial Gyrase-DNA Complex. *J. Med. Chem.* **1995**, *38*, 408–424. [[CrossRef](#)]
19. TerHune, T.N.; Skogerboe, T.L.; Shostrom, V.K.; Weigel, D.J. Comparison of pharmacokinetics of danofloxacin and enrofloxacin in calves challenged with *Mannheimia haemolytica*. *Am. J. Vet. Res.* **2005**, *66*, 342–349. [[CrossRef](#)]
20. Barrón, D.; Irlés, A.; Barbosa, J. Prediction of electrophoretic mobilities in non-aqueous capillary electrophoresis: Optimal separation of quinolones in acetonitrile–water media. *J. Chromatogr. A* **2000**, *871*, 367–380. [[CrossRef](#)]
21. Lizondo, M.; Pons, M.; Gallardo, M.; Estelrich, J. Physicochemical properties of enrofloxacin. *J. Pharm. Biomed.* **1997**, *15*, 1845–1849. [[CrossRef](#)]
22. Romañuk, C.B.; Manzo, R.H.; Linck, Y.G.; Chattah, A.K.; Monti, G.A.; Olivera, M.E. Characterization of the Solubility and Solid-State Properties of Saccharin Salts of Fluoroquinolones. *J. Pharm. Sci.* **2009**, *10*, 3788–3801. [[CrossRef](#)] [[PubMed](#)]
23. Xu, Y.; Jiang, L.; Mei, X. Supramolecular structures and physicochemical properties of norfloxacin salts. *Acta Crystallogr. Sect. B Struct. Sci. Cryst. Eng. Mater.* **2014**, *70*, 750–760. [[CrossRef](#)] [[PubMed](#)]
24. Surov, A.O.; Manin, A.N.; Voronin, A.P.; Drozd, K.V.; Simagina, A.A.; Churakov, A.V.; Perlovich, G.L. Pharmaceutical salts of ciprofloxacin with dicarboxylic acids. *Eur. J. Pharm. Sci.* **2015**, *77*, 112–121. [[CrossRef](#)]
25. Banerjee, R.; Bhatt, P.M.; Ravindra, N.V.; Desiraju, G.R. Saccharin Salts of Active Pharmaceutical Ingredients, Their Crystal Structures, and Increased Water Solubilities. *Cryst. Growth Des.* **2005**, *5*, 2299–2309. [[CrossRef](#)]
26. Dolomanov, O.V.; Bourhis, L.J.; Gildea, R.J.; Howard, J.A.K.; Puschmann, H. OLEX2: A complete structure solution, refinement and analysis program. *J. Appl. Crystallogr.* **2009**, *42*, 339–341. [[CrossRef](#)]
27. Sheldrick, G.M. SHELXT-Integrated space-group and crystal-structure determination. *Acta Crystallogr. Sect. A Found. Adv.* **2015**, *71*, 3–8. [[CrossRef](#)]
28. Spek, A.L. Structure validation in chemical crystallography. *Acta Cryst.* **2009**, *D65*, 148–155.
29. Glomme, A.; März, J.; Dressman, J.B. Comparison of a Miniaturized Shake-Flask Solubility Method with Automated Potentiometric Acid/Base Titrations and Calculated Solubilities. *J. Pharm. Sci.* **2005**, *94*, 1–16. [[CrossRef](#)]
30. Shaibat, M.A.; Casabianca, L.B.; Wickramasinghe, N.P.; Guggenheim, S.; de Dios, A.C.; Ishii, Y. Characterization of Polymorphs and Solid-State Reactions for Paramagnetic Systems by <sup>13</sup>C Solid-State NMR and ab Initio Calculations. *J. Am. Chem. Soc.* **2007**, *129*, 10968–10969. [[CrossRef](#)]
31. Mesallati, H.; Umerska, A.; Tajber, L. Fluoroquinolone Amorphous Polymeric Salts and Dispersions for Veterinary Uses. *Pharmaceutics* **2019**, *11*, 268. [[CrossRef](#)] [[PubMed](#)]
32. Löbmann, K.; Laitinen, R.; Grohgan, H.; Strachan, C.; Rades, T.; Gordon, K.C. A theoretical and spectroscopic study of co-amorphous naproxen and indomethacin. *Int. J. Pharm.* **2013**, *453*, 80–87. [[CrossRef](#)] [[PubMed](#)]
33. Gunasekaran, S.; Anita, B. Spectral investigation and normal coordinate analysis of piperazine. *Indian J. Pure Appl. Phys.* **2008**, *46*, 833–838.
34. Karanam, M.; Choudhury, A.R. Structural Landscape of Pure Enrofloxacin and Its Novel Salts: Enhanced Solubility for Better Pharmaceutical Applicability. *Cryst. Growth Des.* **2013**, *13*, 1626–1637. [[CrossRef](#)]

